Water vapor stable isotope memory effects of common tubing materials

Alexandra L. Meyer[1], Lisa R. Welp[1]

[1]Department of Earth, Atmospheric, and Planetary Sciences, Purdue University, West Lafayette, 47906, United States

5   *Correspondence to: almeyer269@gmail.com or lwelp@purdue.edu*

10

15

20

25

30

Atmospheric
Measurement
Techniques
Discussions

Open Access

EGU

Abstract. Water molecules in vapor exchange with water molecules sticking to surfaces of sampling tubing, and
exchange rates are unique for each isotopologue and tubing material. Therefore, tubing walls take some time to reach
isotopic equilibrium with a new vapor isotopic signal, creating a memory effect observed as attenuation time for signal
propagation in continuous laser-based stable water vapor isotope measurement systems. Memory effects in δD and
$\delta^{18}O$ measurements can limit the ability to observe fast changes, and because δD and $\delta^{18}O$ memory are not identical,
this introduces transient deuterium excess (D-excess, defined as $\delta D - 8* \delta^{18}O$) artifacts in time-varying observations.
A comprehensive performance comparison of commonly-used tubing material water exchange properties has not been
published to our knowledge. We compared how a large isotopic step change propagated through five tubing materials,
PFA, FEP, PTFE, HDPE, and copper, at two different temperatures and an air flow rate of 1.1 L min^{-1} through
approximately 100 feet (~30.5 m) of $^{1}/_{4}$ inch (6.35 mm) outer diameter (OD) tubing. All tubing materials performed
similarly to each other in terms of attenuation times regardless of temperature. While inner diameter and length of
tubing affect lag times of signal propagation, they don't change the shape of the attenuation curve or the attenuation
times. This indicates that the speed of isotopic equilibrium of the tubing walls can be described as a first order chemical
reaction controlled by the concentration of reactive surface sites rather than the total number of sites. Likewise, use of
a high-surface area particle filter at this air flow rate did not affect the speed of the isotopic signal attenuation.
However, the addition of a mass flow meter did affect the speed of the attenuation, and we recommend investigating
the influence of similar devices during measurement inlet and system design. Our results show that plastic tubing
materials are not inferior to copper in terms of isotopic memory under these conditions, and they are easier to work
with and are less expensive than copper. Users are still advised to maximize air flow rates through both analyzer and
tubing to minimize memory effects especially when accurate time-varying deuterium-excess measurements are
required.

1 Introduction

In situ laser absorption spectroscopy of water vapor isotopologues has risen in use over the last decade and a half
enabling fast, continuous isotopic measurements (Webster and Heymsfield, 2003; Lee et al., 2005; Griffith et al.,
2006; Kerstel et al., 2006). All experimental setups inherently attenuate signal variability due to mixing in the analyzer
optical cavities and molecular water interactions with surfaces inside the inlet and analyzer system, especially when
different H_2O_v concentrations lead to wetting and drying of the tubing walls. The timescale for signal attenuation can
vary greatly based on a wide range of tubing materials, air flow rates, temperatures, and pressures used (Sturm and
Knohl, 2010; Griffis et al., 2010; Schmidt et al., 2010; Tremoy et al., 2011; Aemisegger et al., 2012; Galewsky et al.,
2016). As condensation in tubing is a concern due to the possibility of liquid-vapor fractionation, many installations
heat the tubing above ambient temperature, use a critical orifice at the tubing inlet to drop pressure in the lines, or do
both in order to keep the vapor in the tubing above the dew point (e.g. Griffis et al. 2010; Luo et al. 2019).

Initially, a plastic coated aluminum Synflex tubing (also known as Dekabon or Dekoron) commonly used in the
carbon dioxide and water eddy covariance flux community was used in water vapor isotope experiments (Lee et al.,
2005; Gupta et al., 2009; Tremoy et al., 2011), but it was found to greatly attenuate the water isotopic signals. Testing
in various labs has led to the adoption of plastic or solid metal tubing, but the details of the experimental results are

70   sparce (Sturm and Knohl, 2010; Griffis et al., 2010; Schmidt et al., 2010; Tremoy et al., 2011). Commonly used tubing material types now include copper and several types of plastic tubing including polytetrafluoroethylene (PTFE, commonly referred to as Teflon) (Sturm and Knohl, 2010; Griffis et al., 2010), perfluoroalkoxy (PFA) (Schmidt et al., 2010; Tremoy et al., 2011), fluorinated ethylene propylene (FEP) (Luo et al., 2019), and high-density polyethylene (HDPE) (Griffis et al., 2010). Fluorinated polymers (FEP, PFA, and PTFE) are commonly used as transfer lines in

75   chemical, pharmaceutical, food processing, and oil and gas industries because of their chemical- and weather-resistance, as well as their non-stick and dielectric properties (Chemours, 2018). These materials have found favor in water vapor isotope applications for the same reasons.

Air tubing choices are important because materials may have different affinities, or degree of attraction, for the isotopologues of water. This causes a delay in the speed at which the isotopologues move through the tubing, called

80   the memory effect. Memory may be lessened at higher temperatures and faster air flow rates (Griffis et al., 2010). The memory effect is strongest for δD compared to $\delta^{18}O$ due to hydrogen bonding slowing tubing wall exchanges (Sturm and Knohl, 2010; Griffis et al., 2010; Schmidt et al., 2010). This can result in false D-excess (defined as $\delta D - 8* \delta^{18}O$) anomalies and is important to minimize when D-excess signals are interpreted as fast temporal-scale atmospheric signals (Managave et al., 2016; Galewsky et al., 2016; Sodemann et al., 2017; Salmon et al., 2019).

85   It is important to minimize isotopic wall effects in the intake tubing lines and other pre-analyzer in-line elements to minimize signal attenuation. Four studies previously reporting memory effects of tubing types tested a maximum of three materials at a time and are summarized in Table 1 (Sturm and Knohl, 2010; Griffis et al., 2010; Schmidt et al., 2010; Tremoy et al., 2011). Most concluded that Dekabon was not suitable for water isotope applications but varied in which tubing was preferred across applications. The National Ecological Observatory Network (NEON)

90   selected a newer material, FEP for their monitoring installations which has not been widely used in reported studies (Luo et al., 2019). In this study, we tested five of the commonly used and reported best tubing types under identical conditions at two different temperatures to determine which tubing type and temperature combination produces the least isotopic signal attenuation.

Table 1. Literature findings

Author, year	Materials Tested	Isotopes Used/Goals	Result
*Schmidt et al. 2010	Stainless, PFA, and Dekabon	δD and $\delta^{18}O$, Analyzer calibration	PFA better than SS. Both better than Dekabon.
*Sturm and Knohl 2010	PTFE and Dekabon	δD and $\delta^{18}O$, Analyzer characterization	PTFE better than Dekabon
Griffis et al. 2010	"Natural colored" HDPE, Teflon (PTFE), and Dekabon	δD and $\delta^{18}O$, $\delta^{18}O$ measurements of evapotranspiration in eddy covariance setups	HDPE equal or slightly better than PTFE. Both much better than Dekabon.
Tremoy et al. 2011	PFA and Dekabon	δD, $\delta^{18}O$, and D-excess, Analyzer characterization and D-excess measurements	PFA better than Dekabon

Atmospheric
Measurement
Techniques

Discussions

Open Access

EGU

95   *Indicates experimental details and results of source-switching experiments are included in the peer-reviewed materials.

2 Methods

In this study, we tested PFA, FEP, PTFE, HDPE and copper at ambient and elevated temperature using self-regulating heat tape switching between two isotopically distinct vapor sources to examine memory effects during water vapor
100   stable isotope measurements.

2.1 Analyzer

A Los Gatos Research, Inc. (LGR) Triple Water Vapor Isotope Analyzer (TWVIA) Off-Axis Integrated-Cavity-Output Spectroscopy system (OA-ICOS) analyzer was used for testing. The air flow rate through the analyzer was 0.1 L min^{-1} (slow analyzer) or 0.2-0.3 L min^{-1} (fast analyzer) run in standard mode at ~40 torr. Twenty-second one-sigma
105   values for δD and δ^{18}O at the slow analyzer speed with in-line elements were 0.5‰ and 0.12‰, respectively, over 4.5 hours at approximately 8,800 ppm. For the fast analyzer without in-line elements, these values were 0.3‰ for δD and 0.10‰ for δ^{18}O over 2.3 hours at ~9,200 ppm.

2.2 Experimental Setup

The memory effect of the tubing material was tested by switching between two sources of moist air with different
110   isotopic values but nearly identical water vapor mixing ratios (~9,000 ppm) (Table S1). We chose to hold water vapor mixing ratios constant to minimize additional effects of moistening and dehydrating the tubing walls, but rather isolate any differences in the rate of exchange of the isotopologues. It also eliminated the need to correct the isotopic measurements for the mixing ratio dependence of the analyzer. A LiCor model LI-610 portable dew point generator (DPG) was used to create a vapor of approximately -170‰ δD, -21.3‰ δ^{18}O, and -1.8‰ D-excess from water at 5
115   degrees C for the slow analyzer tests. The second vapor of approximately -34‰ δD, -3.7‰ δ^{18}O, and -3.2‰ D-excess was produced by a Los Gatos Research Water Vapor Isotope Standard Source (WVISS) for the slow analyzer tests. For the fast analyzer tests, these values were approximately -179‰ δD, -22.1‰ δ^{18}O, and -1.5‰ D-excess from the DPG and approximately -27‰ δD, -3.1‰ δ^{18}O, and -2.8‰ D-excess from the WVISS. DPG-generated vapor isotopic values for the experiments became isotopically enriched over time as water evaporated from the liquid reservoir
120   following Rayleigh fractionation. Isotopic δD and δ^{18}O transitions were normalized to a 0 to 1 scale to compare across experiments and adjust for source water and analyzer drift over time. Five replicate switches were completed for each experiment where the vapor sources switched approximately every 64 minutes giving sufficient time to reach a new isotopic equilibrium.

For each experiment, the WVISS programming and internal valve system controlled the switching between the DPG
125   output connected to the WVISS inlet port and the WVISS (Figure 1) output to the WVIA. The WVISS was connected to the analyzer by approximately 100 feet (~30.5 m) long sections of $^1/_4$ inch (6.35 mm) outer diameter (OD) test tubing for the main experiments. Additional tests were done with two short pieces of PTFE (53 inch or 1.35 m thick-walled PTFE; 54 inch or ~1.37 m thin-walled PTFE) to quantify sensitivity to tubing length and interior diameter.

Tubing inner diameters (ID, summarized in Table S1) were $3/16$ inch (~4.76 mm) with the exception of HDPE, thick-walled FEP, and thick-walled short PTFE, which were $1/8$ inch (~3.18 mm) ID. The thin-walled FEP tubing was pieced together using three stainless-steel Swagelok unions, but this is not expected to affect the results significantly. Tubing and self-regulating heat tape (EASYHEAT ADKS-0500, 100-foot roof and gutter de-icing kit) were wrapped in either flexible foam tape (HDPE, PTFE, thick-walled FEP; AP/Armaflex TAP 18230 insulation tape) or rigid foam pipe insulation (copper, thin-walled FEP, PFA; Tundra brand $1/2$ inch wall). During heated tubing tests, the tubing was allowed to warm up at least an hour to ~60°C prior to measurements to let the tubing moisture equilibrate to the elevated temperature and minimize the effects of degassing water molecules adhered to the tubing from previous experiments.

Air flow rates through the tested tubing were 1.1 ± 0.1 L min^{-1}. Slight variations in flow between experiments within measurement uncertainty may have occurred. WVISS and DPG internal pumps push humid air through the test tubing while an external pump (KNF pump, model N920-2.08) pulls air through the analyzer. The WVIA itself regulates the outflow to maintain a constant internal pressure. Dwyer rotameters (Model number VFB-65-SSV) were used to monitor air flow rates directly upstream of the external pump, at the excess flow from the WVISS output and the WVIA inlet, and between the DPG and WVISS. An Omega mass flow meter (MFM, 0–30 L min^{-1} range, model FMA1826A) was used to validate rotameter air flow rates prior to the experiments. Air flow rates do not add up, but the Omega uncertainty and readability were 0.45 L min^{-1} and 0.15 L min^{-1}, respectively. In addition, the Omega readout only displays to one decimal, which may have contributed to the differences. During slow analyzer testing, the MFM was located directly downstream of the WVISS, prior to the test tubing. A brass inline particulate filter with a stainless steel 2-micron pore size insert (Swagelok part no. B-4F-2) was used just upstream of the tee between the vent and analyzer. In the fast analyzer tests, the Omega, filter, and associated connectors were removed and just the intake tubing and vent before the analyzer remained.
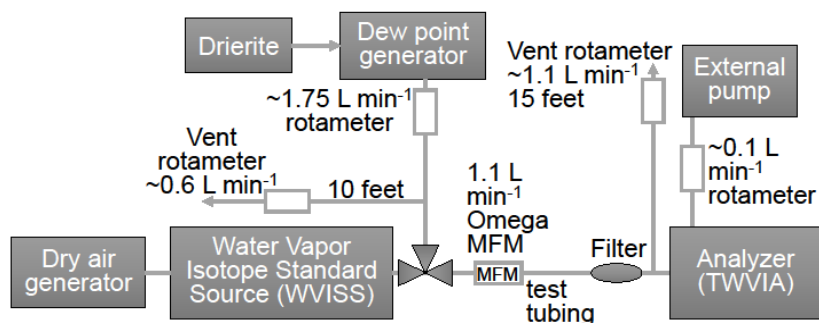

Figure 1. Slow analyzer instrument setup for memory effect tests. The WVISS controls switching between WVISS air and dew point generator air (depicted here as a 3-way valve), which is passed through test tubing connected to the analyzer. Air flow rates next to the rotameters were measured using the MFM as the pressure influences absolute air flow rates. In fast analyzer tests, analyzer flow was 0.2-0.3 L min^{-1} and the Omega mass flow meter and filter were removed. Air flow rates do not add up but are within uncertainty and repeatability metrics of the Omega.

2.3 Data Analysis

Isotopic values were measured at 1 Hz and a 20 s running mean was applied to reduce noise while minimizing

160 smoothing over signal changes (Figure S1). This was done prior to normalization of the y-axis for comparison between tubing types. For δD and $\delta^{18}O$, data was normalized to represent the enriched (maximum delta value, or 1) to depleted (minimum delta value, or 0) transition. Maximum δ values were the average of 10 seconds on either side of the maximum and the average minimum δ value over 1800–2000 seconds after the source switch. In the fast analyzer experiment with short thin PTFE (where the lag time, discussed later in the methods, is 0 seconds) the maximum delta

165 value was used. D-excess was calculated without normalization because the shape of the attenuation curve is different. We calculated the average δ value over 3400–3600 seconds and subtracted that value from all data points to adjust for small changes in D-excess source waters between replicates. These averaging intervals were used to calculate source vapor sample averages given in Table S1 and summarized in section 2.2.

Replicates were screened based on successful WVISS/DPG switching and consistent water vapor concentrations

170 ensuring that vapor generators were operating properly. Only one replicate was discarded, a fast analyzer short thin PTFE experiment when the Drierite was depleted after the 4th replicate. The replicates of each experiment were averaged to produce the curves in Figure 2. From this average of replicates, attenuation time thresholds were calculated and time-varying standard deviation was used to report uncertainty of the thresholds. This standard deviation was added or subtracted from the averaged curve to calculate the range of attenuation time uncertainty (Figure 3).

175 Analysis focuses only on the isotopically enriched-to-depleted switch due to an isotopic signal artifact in the depleted-to-enriched switch created by pressure changes in the system during a purge cycle when the WVISS interval initiates. However, we did not see a difference in attenuation times in either direction (Figure S2). While Aemisegger et al. (2012) found the enriched-to-depleted switch exhibited longer attenuation times, this was likely due to the associated decrease in water vapor mixing ratio of the sources in their experiment which did not occur here.

180 Our measurements allow us to quantify the tubing memory, adjusting for signal lag time. Memory effects are analogous to a low-pass filter (e.g. Zannoni et al., 2022) with an approximately exponential transition (Sturm and Knohl, 2010; Schmidt et al., 2010; Aemisegger et al., 2012). E-folding time corresponds to 1/e of the signal transition remaining to reach a new value. In this study, we have chosen to estimate attenuation times of approximately 1τ (~63%) and 3τ (~95%) completion of the switch to the next δD and $\delta^{18}O$ value, denoted as $t_{63\%}$ or $t_{95\%}$ respectively

185 (Schmidt et al., 2010). We chose not to fit exponential curves to extract an e-folding time, because the measured attenuation curves follow more of a reverse sigmoidal shape. Signal propagation is also delayed by the time it takes air to move through the tubing from the WVISS and mixing inside the analyzer, denoted as lag time. Lag time is controlled by the air flow rate through the instrument and optical cavity size, and intake tubing ID and air flow rate (Schmidt et al., 2010).

190 D-excess signals of the source transitions have a very different shape and memory must be quantified differently. Previous studies reported that δD signals take longer to equilibrate with the surface of tubing materials due to interactions with the tubing walls and hydrogen bonding compared to $\delta^{18}O$ signals (Sturm and Knohl, 2010; Griffis et al., 2010; Schmidt et al., 2010; Aemisegger et al., 2012). This difference leads to a D-excess transition that is not a monotonic near-exponential transition like $\delta^{18}O$ and δD, but rather has a transient positive anomaly until the δD signal

Atmospheric
Measurement
Techniques
Discussions

195   propagation catches up to δ^{18}O. The average difference between the beginning and ending D-excess values was only 1.4‰ for both fast and slow analyzer settings, while the transient peaks reached ~20‰ for slow analyzer air flow and ~15‰ for fast analyzer air flow. The direction of the D-excess transient peak depends on the direction of the isotopic signal switch. In the enriched-to-depleted transition, the enriched δD signal is retained on the tubing walls creating a transient, positive anomaly in D-excess while approaching equilibrium. However, in a depleted-to-enriched transition,

200   the depleted δD signal has been preserved on the tubing walls creating a negative D-excess anomaly during isotopic equilibration. An e-folding time value cannot capture the features of the D-excess transitions. The metric chosen to measure completion in D-excess transitions is a 3‰ threshold within the new equilibrium value, determined by the average over 3400–3600 s. This threshold is a conservative threshold of analyzer precision of D-excess measurements. An Allen plot of the slow analyzer variance estimates D-excess precision of ±1.5‰ (Figure S1), while fast analyzer

205   variance estimates ±1.1‰.

To compare the attenuation curves across experiments, we adjusted for differences in lag times that occur due to different tubing inner volumes and air flow rates. Smaller tubing IDs, faster tubing and analyzer air flow rates, and shorter tubing lengths will all shorten lag times associated with a measurement. Lag times were calculated via breakpoint analysis to determine the point where slope changes. We created a linear model using the first 30 s (62 s

210   for fast analyzer tests) of data after the source switched, then utilizing the "segmented" function in R's "segmented" package on the time series (Muggeo, 2022). We estimate the uncertainty of the breakpoint lag estimate to be on the order of a few seconds. Average lag times for 100 foot tubing with slow analyzer experiments were 51 s for thin-walled tubing (with and without filter) and 35 s for thick-walled tubing. All short tubing slow analyzer lag times were 20 s. For the fast analyzer tests, the average lag time for the long tubing was 30 s, and 0 s for the short tubing. Short

215   and thick-walled tubing types have been lag adjusted to their long and thin-walled counterparts for all figures.

3 Results

The mean attenuation curves in Figure 2 were used to compare tubing experiments and quantify $t_{95\%}$ and $t_{63\%}$ for δD and δ^{18}O, or $t_{3‰}$ for D-excess which are summarized in Figure 3. There is remarkable agreement between tubing types for δD or δ^{18}O, and little-to-no difference between heated and unheated experiments (Figures 2 and 3). Figure 2

220   compares all tubing material types at two temperatures over the full 1-hour experiment length (panels a, c, and e) and the first 600 s after the source switch (panels b, d, and f). Normalized δ^{18}O signals for all tested tubing types reached the $t_{95\%}$ value by 600 seconds (10 minutes) and the $t_{63\%}$ value by 2 minutes in the slow analyzer setting (Figure 2). For δD, $t_{95\%}$ doesn't occur until ~850 seconds (~14 minutes) and 3 minutes for $t_{63\%}$. Figure 2, panels b and d also show the mean signal transition for the other isotopologue in grey for direct comparison showing the longer transition times

225   for δD compared to δ^{18}O. For D-excess, the transition response curves and times to achieve 3‰ within the final value are similar regardless of tubing type and temperature and are typically much longer than the $t_{95\%}$ times for δD or δ^{18}O. Under the fast analyzer setting (Figure 4 panels a and c), measured transitions occur much sooner for both isotopes, with signals reaching $t_{95\%}$ and $t_{63\%}$ levels within ~30 s and 18 s for δ^{18}O, and 90 s and 21 s for δD.
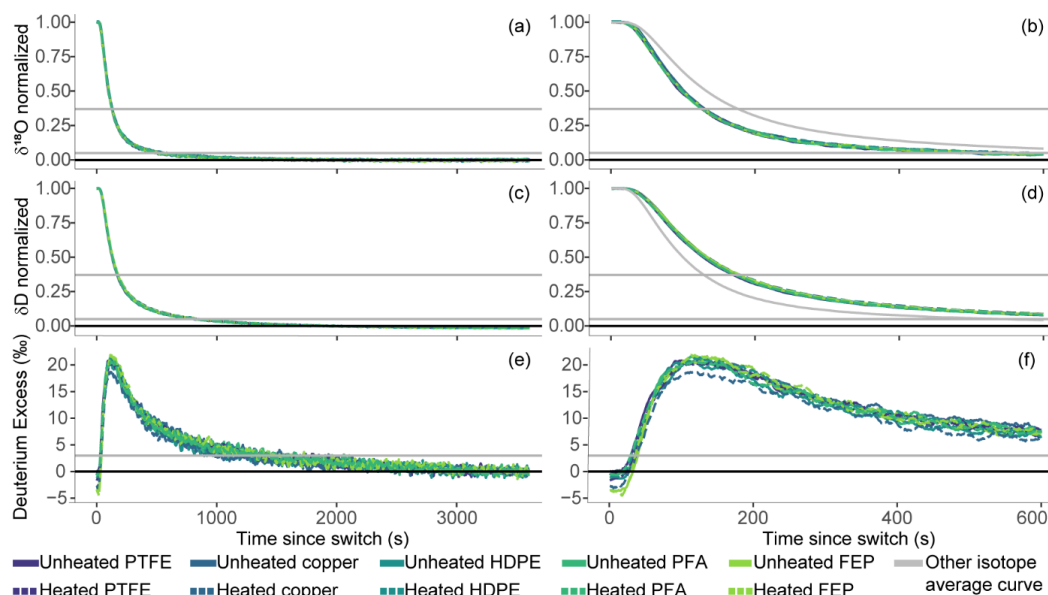
Figure 2. Mean attenuation curves for enriched-to-depleted transitions of five replicates of each tubing type for δ^{18}O (a, b), δD (c, d), and D-excess (e, f) plotted as time since source switch. The first column (panels a, c, and e) depicts the full 1-hour experiment length, while the second column (panels b, d, and f) depict the first 600 s after the source switch. Solid lines indicate unheated experiments of thin-walled tubing, while dashed lines indicate heated experiments. For δD, δ^{18}O, and D-excess, unheated and heated tubing performances are similar with no clear optimal material or temperature under these conditions. A grey curve in panel b shows δD for comparison with δ^{18}O in color and the grey curve in panel d shows δ^{18}O for comparison with δD in color. To compensate for small differences in isotopic values between experiments, δD and δ^{18}O are normalized from 0–1 with zero at the start of the source switch and 1 at the final value after 1 hour, and D-excess is adjusted to end at 0‰ for each experiment. Gray horizontal lines indicate thresholds of 95% and 63% transition completion for δD and δ^{18}O, and 3‰ for D-excess, while a black line indicates 100% completion for all isotopes.
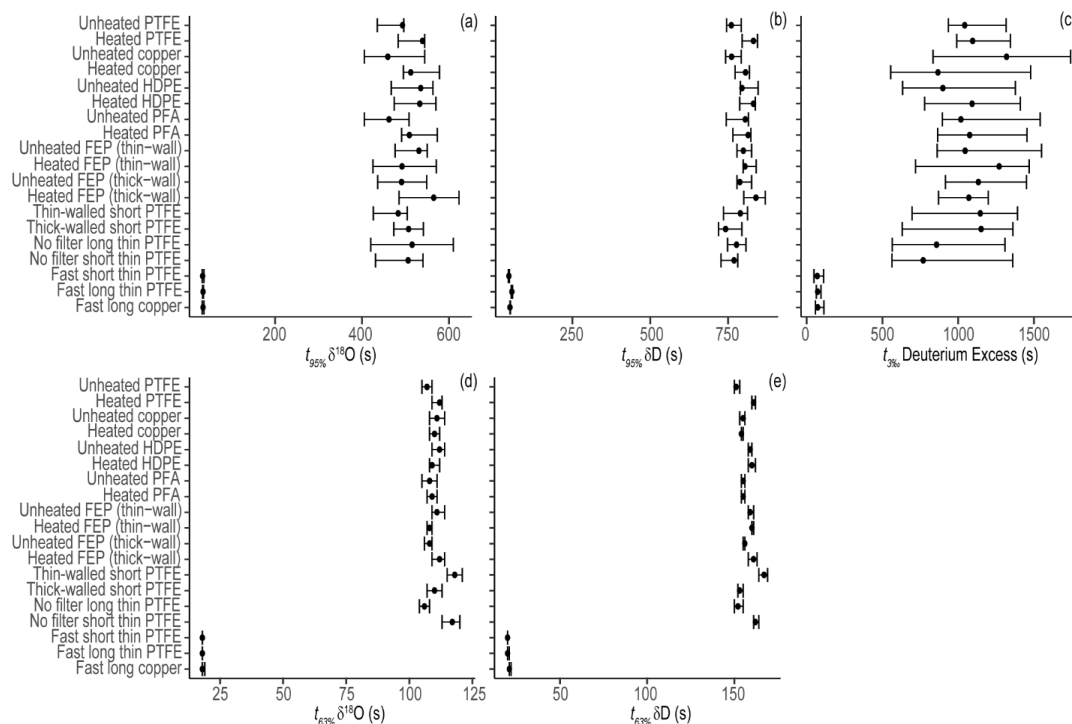
Figure 3. Mean attenuation times $t_{95\%}$, $t_{63\%}$, and uncertainties for all experiments for δ^{18}O (a), δD (b), and $t_{3‰}$ for D-excess (c) estimated from the replicates organized by tubing type and appearance in the discussion. In this figure, lag times have been subtracted from attenuation times. For δD, δ^{18}O, and D-excess, unheated and heated tubing performances are similar within uncertainty with no clear optimal material or temperature among those tested.

For all tubing material types and conditions under the same analyzer air flow rate, unheated and heated $t_{95\%}$, $t_{63\%}$, and $t_{3‰}$ times are similar (Figure 3). Under slow analyzer settings, the measured $t_{95\%}$ values for δ^{18}O range from 459–565 seconds, with uncertainties ranging from 405–623 seconds. Measured values of $t_{95\%}$ for δD range from 742–839 seconds, with uncertainties ranging from 707–869 seconds. Under fast analyzer settings, the measured $t_{95\%}$ values for δ^{18}O range from 33–34 seconds, with uncertainties ranging from 32–36 seconds. Measured values of $t_{95\%}$ for δD range from 46–56 seconds, with uncertainties ranging from 45–58 seconds. Because of the shape of the attenuation curves, we report $t_{63\%}$ values also because they may have different sensitivity to tubing differences than the end-of-experiment tails. For slow analyzer settings, $t_{63\%}$ values range from approximately 106–118 s and 152–167 s for δ^{18}O and δD respectively, with uncertainty adding a couple more seconds to those ranges. Fast analyzer $t_{63\%}$ values are ~18 s and ~ 20 s. Finally, $t_{3‰}$ values for D-excess range from 550-1320 seconds in the slow analyzer settings, while uncertainty has a large range from 550–1743 seconds, overlapping both δD and δ^{18}O $t_{95\%}$ ranges. The longest amount of time to the D-excess $t_{3‰}$ for 100-foot tubing under slow analyzer settings was 1320 seconds, or 22 minutes, while the shortest

260   is 12.8 minutes, while values dropped to ~70 s under fast analyzer settings. A second attenuation metric for judging

D-excess is not appropriate because of the curve shapes.
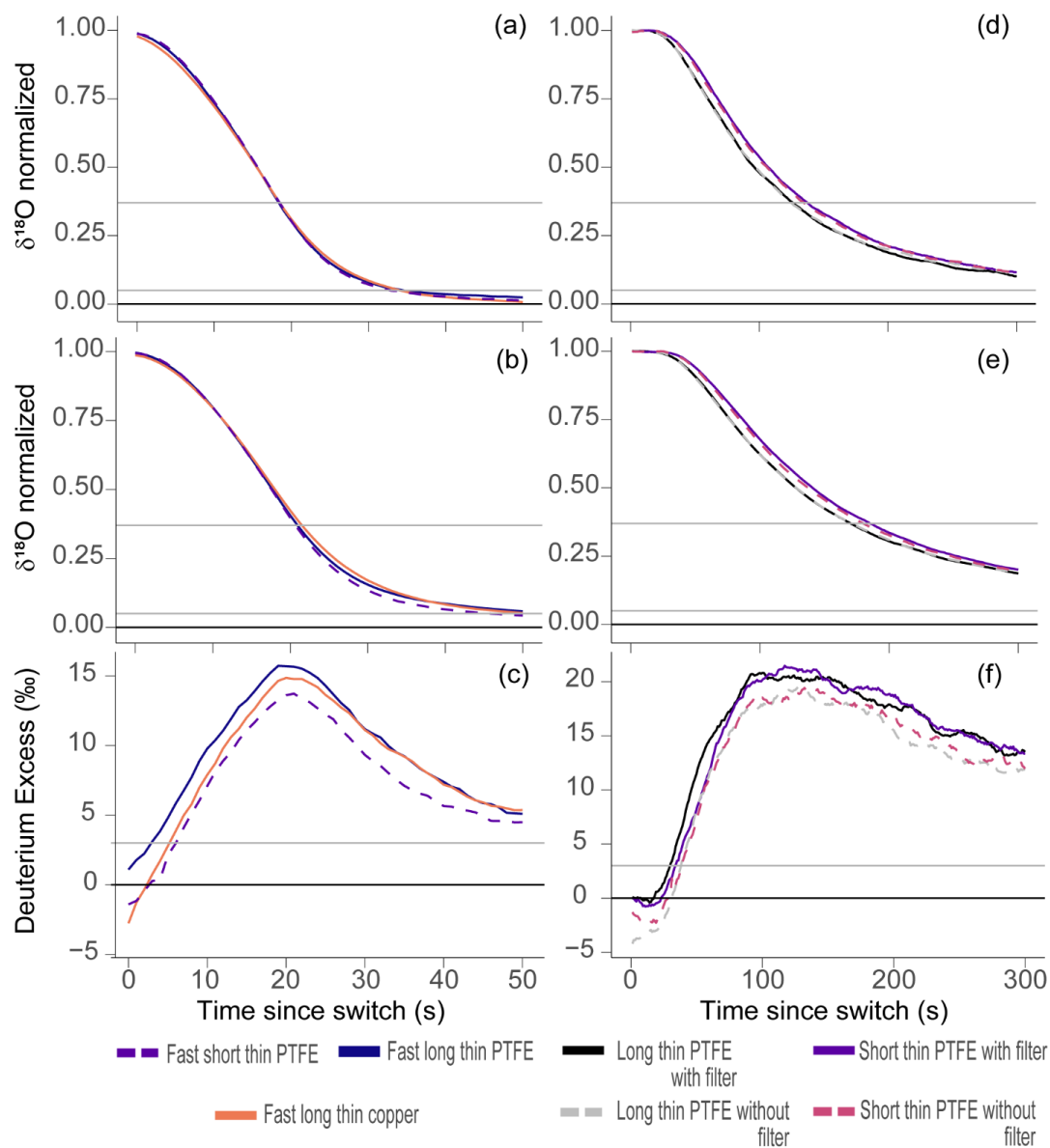
Figure 4. Mean attenuation curves for enriched-to-depleted transitions comparing the influence of analyzer air flow
265   rate, tubing length and in-line element use for $\delta^{18}O$ (a, b), δD (c, d), and D-excess (e, f) plotted as time since source
switch. The first column (panels a, c, and e) depicts results at the faster air flow rate with the long and short PTFE
without in-line elements, as well as a long copper experiment to test tubing length and material type differences. The

Atmospheric
Measurement
Techniques

Open Access

EGU

Discussions

second column (panels b, d, and f) depicts results at the slower air flow rate with the short and long PTFE with and without the presence of a filter. Solid lines indicate experiments with long tubing lengths, while dashed lines indicate experiments with short tubing lengths. With and without filter tests are similar in terms of δD and δ^{18}O, but separate slightly in D-excess and between short and long tubing lengths. Similarly, under fast analyzer air flow settings, tested tubing types are similar in terms of δD and δ^{18}O, but separate slightly in D-excess. To compensate for small differences in isotopic values between experiments, δD and δ^{18}O are normalized from 0–1, and D-excess is adjusted to end at 0‰ for each tubing experiment. Gray horizontal lines indicate thresholds of 95% and 63% completion for δD and δ^{18}O, and 3‰ for D-excess, while a black line indicates 100% completion for all isotopes. Short tubing lengths have been lag adjusted to their long counterparts.

Properties affecting transit time through the tubing, referred to here as lag time, like tubing length and inner diameter, do not appear to influence the $t_{95\%}$, $t_{63\%}$, and $t_{3‰}$ values after lag-adjustment for δD, δ^{18}O, and D-excess (Figure 3 and S3). Times for isotopic equilibration were similar for both thick- and thin-walled tubing materials as well as long and short tubing (Figures 4d-f and S3). The slight visual difference between short and long PTFE tubing lengths may be due to slight variations in flow control conditions between the short and long tubing experiments (Figure 4). Under identical air flow conditions, the reverse sigmoid shapes of the isotopic transitions are similar. Also, the presence or absence of the filter in the 1 L/min flow section does not change the $t_{95\%}$ or $t_{63\%}$ results for δD and δ^{18}O (Figure 4d-f). However, there is a slight visual difference in D-excess between experiments with and without a filter that is at least partially due to variability in the D-excess of source waters between the experiments.

Predictions of tubing material performance under different sets of air flow conditions can be made based on material properties. Hydrophobic materials that are nonpolar and have a high relative permittivity (also known as the dielectric constant, or a material's ability to prevent electrical fields from forming) are ideal for water vapor isotope studies as polar water molecules are affected by and can induce electric fields (Aemisegger et al., 2012). As previously discussed, δD signals are slowed when traveling past the surface of a material when compared to δ^{18}O signals, due to increased hydrogen-bonding interactions with tubing walls. Limiting these interactions should lead to reduced isotope signal attenuation times. Specifications vary by manufacturer and material purity, but in general, FEP and PTFE materials have the least amount of water absorption of the tubing types we tested (Table 2). Metals have a relative permittivity value of ~1 due to their sea of electrons, which in this case move to interact with the polar water molecules. Larger values of relative permittivity are better in this case, as water vapor molecules will not be as attracted to the material. HDPE, FEP and PTFE have the highest ability to prevent electrical fields. FEP and PTFE may be expected to have the shortest isotopic attenuation times. At the air flow rates we tested, the effects of these relative permittivity differences on isotope attenuation times were not noticeable but might be confirmed by testing at lower air flow rates through intake tubing and faster analyzer internal flow rates.

Table 2. Material properties of tubing type options and their water absorption percentages and relative permittivity values.

Atmospheric
Measurement
Techniques

Open Access

EGU

Discussions

Material	Water absorption %	Relative Permittivity (Dielectric constant) @ 1 MHz (ε_r)
FEP	<0.01[1]	2.1[2]
PFA	<0.03[1]	2.05–2.06[2]
PTFE	<0.01[1]	2.0–2.1[2]
HDPE	0.10[1]	2.3–2.4[2]
Copper	N/A	~1
Stainless steel	N/A	~1

305   [1] after being submerged for 24 hours (ASTM D570) [2] (Electrical properties of plastic materials, 2021)

4 Discussion

Our study compared five commonly used tubing types to determine whether material and temperature combinations differ in their isotopic memory effects. We also discuss the effects of intake tubing inner diameter and length, the inclusion of in-line elements including the filter and Omega mass flow meter, and analyzer air flow rates through the optical cavity on the attenuation time and shape of the attenuation curves.

4.1 Effects of material type and temperature

We found that for δD and $\delta^{18}O$ there is little-to-no difference between tubing types at these flow rates, humidities, and temperatures (Figures 2 and 3). Our results are consistent with Griffis et al.'s (2010) assertion that HDPE is similar to PTFE. Similarly, Aemisegger et al., (2012) found little difference in attenuation times with varying PFA tubing temperatures.

4.2 Effects of tubing ID and length

Once adjustments were made for the lag times in signal propagation to the analyzer, we found that the tubing dimensions including ID and length had little effect on the isotopic attenuation times (Figure 4 and S3). The ID of the tubing affects the surface area to air volume ratios. If using 100 feet of tubing, there is a 1.5 times decrease in internal surface area and a 2.25 times decrease in volume for the $^1/_8$ inch ID thick-walled tube compared to the $^3/_{16}$ inch ID thin-walled tube. Similarly, a shorter 53-inch thick-walled tube has 34 and 51 times lower internal surface area and volume respectively compared to a 100-foot thin-walled tube, yet the shape of the isotopic attenuation curves remained similar. We see this when comparing thin-walled short and long tubing as well (Figure 4). A 95% shorter length does not lead to a 95% decrease in attenuation times. The similar attenuation curve shape regardless of tubing type and dimensions could be for two reasons. First, the isotopic memory of the analyzer optical cavity and internal plumbing are likely much larger than tubing effects in the flow conditions of the slow analyzer setup. However, even in the faster analyzer flow conditions, there was almost no difference between the short and long thin-walled PTFE

attenuation curves (Figure 4). Second, it could be that the exchange rate of water molecules from the vapor to the inner

330   tubing surface can be considered a first-order kinetic reaction. Therefore, the speed of isotopic equilibration depends on the kinetic rate constant of water adsorption/desorption, the partial pressure of water molecules in the air, and the fraction of water adsorption sites that are out of isotopic equilibrium (see Huang et al., 2016 for rate equations for an analogous set of surface exchange reactions). Due to the dependence on the fraction of sites out of isotopic equilibrium rather than the total number of sites, the speed of signal attenuation to a new equilibrium is not directly dependent on

335   the total length of tubing. There is potential for an indirect effect as the partial pressure of each water isotopologue in the air changes along the length of tubing as a new equilibrium is being established. The isotopic effect of potential pressure differences from the beginning and end of the tubing length are roughly proportional to the change in isotopic delta value that occurs with one tubing volume turnover time. In our experiment, the partial pressure of HDO changes by no more than 4% and $H_2^{16}O$ by no more than 1% from the beginning to the end of 100 feet of tubing with a large

340   step change in vapor isotopic composition. Similar isotopic signal attenuation curves in our experiment imply that the kinetic rate constants for water adsorption/desorption are similar among the materials tested. Further tests under faster analyzer and slower tubing air flow rates would be needed to further validate these results.

4.3 Effects of analyzer air flow rate, filter, and mass flow meter

The air intake flow rate used in this experiment (1.1 L min^{-1}) was fairly slow compared to typical atmospheric

345   observation setups and the flow through the analyzer itself (0.1–0.3 L min^{-1}) was comparable with previously published specifications (Sturm and Knohl, 2010). The air flow rates through the tubing were slow by design to detect relative differences in wall memory effects. Increasing analyzer air flow decreases both the lag time (discussed in Section 4.5), as well as the $t_{95\%}$ and $t_{63\%}$ times, as seen in Figures 3 and 4.

Adding in-line elements in general will increase the expected lag time, so minimizing additional volume or

350   increasing the flow through the tubing is important to allow the new signal to reach the analyzer quickly. Based on non-replicated short-duration switching tests (Figure S4), as well as comparing the difference between fast analyzer with no in-line elements (Figure 4 a-c) to slow analyzer with in-line elements tests (Figures 2 and 4 d-f), the Omega mass flow meter slows the attenuation times, affecting both the lag and lag-adjusted $t_{95\%}$ time. We do not see an effect in lag time or $t_{95\%}$ time when removing only the filter (Figure 4 d-f), so the Omega itself may be the culprit due to its

355   internal volume and/or materials.

4.4 Relative attenuation time differences between δD and δ^{18}O

δD signals have been demonstrated to take longer to isotopically equilibrate with tubing materials than δ^{18}O due to hydrogen bonding interactions with the tubing walls (Sturm and Knohl, 2010; Griffis et al., 2010; Schmidt et al., 2010). This speed difference has been reported as a ratio of attenuation times between the faster δ^{18}O signal and the

360   slower δD signals, and a range of values have been reported. Under air flow conditions of 12 L min^{-1}, Griffis et al. (2010) suggests a 3.5x greater attenuation time for δD signals than δ^{18}O in spectral analysis. Schmidt et al.'s (2010) PFA experiments over a range of water vapor concentrations found a 1.6–3.3x greater $t_{95\%}$ time for δD signals than

Atmospheric
Measurement
Techniques
Discussions

Open Access

EGU

δ^{18}O. We found a 1.57x greater $t_{95\%}$ time value for δD signals than δ^{18}O under slow analyzer conditions and 1.49x greater $t_{95\%}$ value in fast analyzer tests, which is comparable to Schmidt et al. (2010). For $t_{63\%}$, we found a 1.4x greater

365 attenuation time value for δD signals than δ^{18}O under slow analyzer conditions, which is similar to Aemisegger et al.'s (2012) finding that δD signals were 1.5 ± 0.1 times slower than the δ^{18}O signal and Zannoni et al.'s (2022) finding of 1.46x. However, our fast analyzer conditions led to a 1.13x greater e-folding time value, which is smaller than the other estimates. This may be due to a decrease in the relative signal transit times that our analyzer is able to see at the analyzer air flow rate we tested. Our analyzer turnover time is ~8–12 s, while the Aemisegger et al.'s (2012) analyzer

370 had a 2–3 s turnover time. This smaller signal speed difference may also reflect the lack of in-line elements in this test. Neither previously published studies commented on their inlet setup beyond tubing and analyzer air flow rate.

The relative equilibration speed differences in δD and δ^{18}O signals leads to a transient anomaly in D-excess signals (Figure 2 panels e and f, and Figure 4 panels c and f), as the propagation of the depleted δD signal was delayed relative to the depleted δ^{18}O signal (as shown by the gray lines in Figure 2 panels b and d), creating a transient positive

375 anomaly in D-excess before equilibrating. Since the shape of the time-varying D-excess anomaly is different from δD and δ^{18}O, and is not unidirectional, the time to equilibrium must be quantified differently. The time scale for tubing to equilibrate for D-excess was longer than both δ^{18}O and δD. On average it took approximately 17.5 minutes for the transient anomaly to decay to within 3‰ of the ultimate equilibrium value. Smaller isotopic step changes and faster air flow rates will lead to shorter attenuation times.

380 **4.5 Controls of lag time and attenuation curve shape**

Lag times were decreased by shortening the intake tubing and increasing flow through the analyzer (Figure 4). The lag time can be mathematically calculated using the tubing ID, length, and air flow rate through the tubing and analyzer. For the long thin tubing, the calculated lag should be approximately 30 s, with slight variations due to small length differences from 100 feet. The fast analyzer experiments without in-line elements match the calculated lag

385 times. However, in the slow analyzer tests with in-line elements, our observed lag times for the same tubing types are about 20 s slower than the calculated lag times. The difference in lag time is partially due to the inclusion of the in-line elements, which adds approximately 4 s based on their volume estimates. This leads to an unexplained difference of about 17 s for long tubing and 14 s for short tubing between the volumetrically calculated and experimentally observed lag times for the slow analyzer. Differences between expected and observed lag times are likely due to the

390 analyzer's internal volume which could increase lag times in the slow analyzer settings or inaccurate estimates of the internal volume of in-line elements. Uncertainty in the lag time estimate could lead to small differences in attenuation curve offsets.

The overall attenuation curves of the tested tubing material types, lengths, and temperature conditions had effectively the same reverse sigmoidal shape. The slight differences in attenuation curve shapes could be due to small

395 variations in tubing length, uncertainties in lag time corrections, and uncertainties in normalization between experiments. Previous studies approximated the attenuation response as an exponential curve (Sturm and Knohl, 2010; Aemisegger et al., 2012; Schmidt et al., 2010), consistent with the mixing theory for a continuous stirred reactor (Toson et al., 2019). A more appropriate mixing analogy could be the axially dispersed plug flow model (Huang and

Atmospheric
Measurement
Techniques
Discussions

Open Access

EGU

400 Seinfeld, 2019), as this better matches the reverse sigmoid curve we observe. . In this model, there is a bulk flow that has a diffusive 'head' that diverges forwards and backwards from the bulk flow, leading to the observed smoothing of the output signal of an input step-change. We believe this was exaggerated in our experiments due to slow mixing in the analyzer, which adds to the drawn-out leading edge in the early portion of the curve when the signal reaches the analyzer, and that the effects of the slow analyzer air flow also added to the memory effect tail of the later portion of the curve. This 'memory tail' was much more drawn out than the leading edge of the reverse sigmoid curve (Figure

405 2). This, coupled with the fact that there is a difference in attenuation curve shape between δD and $\delta^{18}O$ in the same experimental setup indicates that isotopologue-specific memory on the tubing or analyzer surfaces also affected the attenuation curves. Data presented here suggests that the tubing length or material type at these air flow rates had similar influence on the memory tail near the $t_{95\%}$ values (Figure 2, 3, and 4) in either the fast or slow analyzer. In the fast analyzer settings, varying tubing length and material resulted in $t_{95\%}$ times within error of each other as well

410 (Figure 3 and 4).

5 Implications for measurements

Analyzer signal attenuation times were found to be most sensitive to air flow rates and a mass flow meter, with very small differences among tubing materials. Longer attenuation times smooth signal variability and mask high-

415 frequency features. Therefore, the magnitude and speed of atmospheric signal variability are important considerations when planning for ambient water vapor isotopic measurements.

5.1 Low atmospheric variability measurements

For stationary measurements with one intake and high air flow rates, tubing material selection is not a concern as air advecting past the intake typically has slow isotopic variability compared to tubing attenuation time scales. Conroy et

420 al., (2016) for example, observed vapor on Manus Island, Papua New Guinea changed by 22.3‰ in $\delta^{18}O$ and 154.8‰ in δD, with the largest change being ~25‰ δD over a duration of a few hours. The instant isotopic step change (17.6‰ in $\delta^{18}O$ and 136‰ in δD) in our experiment is extreme compared to typical atmospheric variability. For stationary measurements like the above with low chance of large transient D-excess anomalies, any of the tested tubing materials should be suitable.

425 ### 5.2 High atmospheric variability measurements

For measurements that need high temporal resolution of small atmospheric isotopic variability like flux gradient and eddy covariance setups or airborne observations, extra precautions should be taken. This is also asserted by Aemisegger et al., (2012), who state that the analyzer flow rate and internal tubing have a larger effect on attenuation time than the PFA intake tubing in their experiments. Griffis et al. (2010) used spectral analysis in their eddy

430 covariance experiments to show that tube memory effects weren't a concern for $\delta^{18}O$ signals at tubing air flow rates

of 12 L min^{-1} and analyzer air flow rates of 1.5 L min^{-1}. However, one can't extend that conclusion to slower air flow rates.

Aircraft campaigns are a special concern, as they observe not only at high temporal (and spatial) resolution, but record large isotopic variability as well. Especially when conducting vertical profiles, isotopic compositions can vary

435   by hundreds of per mil in δD. Salmon et al. (2019) found δD signal values ranging from -400 to -175‰ δD within an ~5 minute vertical profile descent between 1200 to 400 m above ground. Similarly, Sodemann et al. (2017) reported flight sections with >200‰ δD variations in under 5 minutes. While data was collected at 1 Hz, their reported data is a 15 second average, which allows them a 975 m horizonal and 75 m vertical resolution (Sodemann et al., 2017), however, that best-case estimate is based on the data averaging interval and does not consider signal attenuation due

440   to tubing isotopic memory or mixing in the optical cavity. Additionally, averaging over long time periods may not remove D-excess memory bias depending on patterns of increasing or decreasing delta values. The wetting and drying of the measurement system during flights with large changes in altitude, and therefore atmospheric humidity, also increase isotopic signal attenuation times but were not quantified here.

In both eddy covariance and aircraft measurement situations, one might consider increasing air flow through the

445   analyzer and intake tubing and shortening the length of tubing from intake pickoff point to the analyzer in slow analyzer flow setups. While high air flow rates can easily be achieved in the air intake main lines in both high-frequency measurement situations, the air flow rate through the analyzer is typically limited by the analyzer design and control software. When tubing or in-line element walls affect the speed at which the isotopes are transmitted from the intake to the optical cavity, signals are effectively low-pass filtered (Zannoni et al., 2022). Therefore, it is also

450   important to minimize the length of tubing from the intake pickoff point to the analyzer to reduce the residence time of air in the low-flow portion of the system. We also suggest testing the effect of any in-line elements like mass flow meters, controllers, or filters on isotopic signal attenuation. The internal materials and geometry of the Omega mass flow meter are currently unknown but had a large effect on isotopic signal attenuation. Though we did not find any materials in this testing that performed particularly poorly, prior research clearly identified Dekabon tubing as

455   unsuitable (Sturm and Knohl, 2010; Griffis et al., 2010; Schmidt et al., 2010; Tremoy et al., 2011). These considerations should maximize D-excess data resolution.

5.3 Liquid water measurements

Liquid water isotope analysis is also plagued by memory effects when samples are converted to the vapor phase for spectral isotopic analysis, especially in applications measuring samples with large isotopic differences in the same

460   batch/run. Common protocols recommend multiple replicate injections and discarding the first few to remove carryover from the previous sample (IAEA, 2009; Penna et al., 2012; Coplen and Wassenaar, 2015). In both OA-ICOS and cavity ring-down spectroscopy, Penna et al. (2012) found that when measuring samples with large isotopic differences, up to eight out of eighteen injections had to be ignored to limit memory effects. When analyzing highly-depleted Antarctic samples ranging from −231.7‰ to −421.1‰ for δD, memory effects of up to 14‰ were found in

465   the first injection compared to the "true" value. Liquid water analysis is one example of a case where air flow rates and temperatures of transfer lines are fixed by the instrument design. Material properties inside the analyzer are

important, but this study finds little difference between commonly used material types. Waiting for equilibrium in the optical cavity may minimize the memory effect, but a time-efficient method to increase sample throughput is to mathematically correct for these repeatable effects rather than attempting to minimize them (Vallet-Coulomb et al., 2021; Hachgenei et al., 2022).

6 Conclusions

Standardizing materials used to measure stable water vapor isotopologues does not seem necessary to make accurate and comparable measurements in most situations as the commonly-used materials tested here perform similarly. We tested the water isotopic exchange properties of PFA, FEP, PTFE, HDPE, and copper. While higher tubing air flow rates will minimize the memory effect, in situations with flow limitations, care needs to be taken to reduce the residence time of air in all portions of the setup including pick-off lines and the analyzer itself. Understanding material limitations can be important in experiments or field situations where there are large isotopic variations over short periods of time in fixed-location observations or over short distances in aircraft observations. This study found that there was not a clearly optimal tubing type or temperature to use in terms of δD, $\delta^{18}O$, and D-excess at our humidity and experimental flow rates. However, we chose to hold water vapor mixing ratios constant to minimize additional effects of moistening and dehydrating the tubing walls. While differences may be found among tubing material types at lower humidity or while changing humidity, these experiments are beyond the scope of this study. We acknowledge that analyzer memory may play a role in our results, and as each individual analyzer is unique, users are advised to test their analyzer for memory effects with no intake tubing. Larger tubing IDs and inclusion of in-line elements will increase lag time, and in-line elements may slow attenuation times as well. Increasing inlet tubing length will also increase lag time, and may lead to relative differences in δD and $\delta^{18}O$ signal propagation due to increased diffusive mixing at the edges of the air plug flow, as described in the axially dispersed plug flow model. As with most decisions, environmental conditions, cost, and preference may affect the type of tubing selected, but researchers must understand the limitations of the air flow conditions and wall effects of their instrumental setups to limit signal memory effects, especially if low air flow rates are a constraint.

Code/Data Availability

All figure data and scripts, as well as an example workup code, are available at https://doi.org/10.4231//H7ZJ-6J45 (Meyer and Welp, 2023).

Author Contributions

ALM and LRW designed the experiments, while ALM conducted them. ALM adapted code (from LRW) and added to it for this project, as well as analyzed data. ALM wrote the manuscript draft, with the section on exchange sites by LRW. ALM and LRW edited the document.

Competing Interests

 The authors declare that they have no conflict of interest.

References

Aemisegger, F., Sturm, P., Graf, P., Sodemann, H., Pfahl, S., Knohl, A., and Wernli, H.: Measuring variations of δ^{18}O and δ^2H in atmospheric water vapour using two commercial laser-based spectrometers: an instrument characterisation study, Atmos. Meas. Tech., 5, 1491–1511, https://doi.org/10.5194/amt-5-1491-2012, 2012.

Chemours: An introduction to Chemours™ fluoropolymers, C–11311. The Chemours Company, FC, LLC, 2018. https://www.chemours.com/en/-/media/files/teflon/intro-to-fluoropolymers.pdf?rev=a43531c7fc5c406d86ced4425f2330b4, last access: 14 July 2022.

Conroy, J. L., Noone, D., Cobb, K. M., Moerman, J. W., and Konecky, B. L.: Paired stable isotopologues in precipitation and vapor: A case study of the amount effect within western tropical Pacific storms, Journal of Geophysical Research: Atmospheres, 121, 3290–3303, https://doi.org/10.1002/2015JD023844, 2016.

Coplen, T. B. and Wassenaar, L. I.: LIMS for Lasers 2015 for achieving long-term accuracy and precision of δ^2H, δ^{17}O, and δ^{18}O of waters using laser absorption spectrometry, Rapid Communications in Mass Spectrometry, 29, 2122–2130, https://doi.org/10.1002/rcm.7372, 2015.

Galewsky, J., Steen-Larsen, H. C., Field, R. D., Worden, J., Risi, C., and Schneider, M.: Stable isotopes in atmospheric water vapor and applications to the hydrologic cycle, Rev. Geophys., 54, 809–865, https://doi.org/10.1002/2015RG000512, 2016.

Griffis, T. J., Sargent, S. D., Lee, X., Baker, J. M., Greene, J., Erickson, M., Zhang, X., Billmark, K., Schultz, N., Xiao, W., and Hu, N.: Determining the oxygen isotope composition of evapotranspiration using eddy covariance, Boundary-Layer Meteorol, 137, 307–326, https://doi.org/10.1007/s10546-010-9529-5, 2010.

Griffith, D. W. T., Jamie, I., Esler, M., Wilson, S. R., Parkes, S. D., Waring, C., and Bryant, G. W.: Real-time field measurements of stable isotopes in water and CO_2 by Fourier transform infrared spectrometry, Isotopes in Environmental and Health Studies, 42, 9–20, https://doi.org/10.1080/10256010500503098, 2006.

Guerrier, S., Balamuta, J., Bakalli, G., Molinari, R., Lee, J., Radi, A., Xu, H., Zhang, Y., and Claussen, N.: avar: Allan variance Version 0.1.1, CRAN [code], https://CRAN.R-project.org/package=avar, 2020.

Gupta, P., Noone, D., Galewsky, J., Sweeney, C., and Vaughn, B. H.: Demonstration of high-precision continuous measurements of water vapor isotopologues in laboratory and remote field deployments using wavelength-scanned cavity ring-down spectroscopy (WS-CRDS) technology, Rapid Communications in Mass Spectrometry, 23, 2534–2542, https://doi.org/10.1002/rcm.4100, 2009.

Hachgenei, N., Vaury, V., Nord, G., Spadini, L., and Duwig, C.: Faster and more precise isotopic water analysis of discrete samples by predicting the repetitions' asymptote instead of averaging last values, MethodsX, 9, 11, https://doi.org/10.1016/j.mex.2022.101656, 2022.

Huang, Y. and Seinfeld, J. H.: A note on flow behavior in axially-dispersed plug flow reactors with step input of tracer, Atmospheric Environment: X, 1, 100006, https://doi.org/10.1016/j.aeaoa.2019.100006, 2019.

Huang, Y.-L., Pellegrinelli, C., and Wachsman, E. D.: Reaction kinetics of gas–solid exchange using gas phase isotopic oxygen exchange, ACS Catal., 6, 6025–6032, https://doi.org/10.1021/acscatal.6b01462, 2016.

IAEA: Laser spectroscopic analysis of liquid water samples for stable hydrogen and oxygen isotopes, International Atomic Energy Agency, Vienna, Germany, 2009.

Kerstel, E. R. T., Iannone, R. Q., Chenevier, M., Kassi, S., Jost, H.-J., and Romanini, D.: A water isotope (^{2}H, ^{17}O, and ^{18}O) spectrometer based on optical feedback cavity-enhanced absorption for in situ airborne applications, Appl. Phys. B, 85, 397–406, https://doi.org/10.1007/s00340-006-2356-1, 2006.

Lee, X., Sargent, S., Smith, R., and Tanner, B.: In situ measurement of the water vapor $^{18}O/^{16}O$ isotope ratio for atmospheric and ecological applications, J. Atmos. Oceanic Technol., 22, 555–565, https://doi.org/10.1175/JTECH1719.1, 2005.

Luo, H., Pingintha-Durden, N., and Smith, D.: NEON sensor command, control and configuration (C3) document: eddy covariance storage exchange (NEON.DOC.000465) Version F, NEON (National Ecological Observatory Network), 71, 2019.

Managave, S., Jani, R., Narayana Rao, T., Sunilkumar, K., Satheeshkumar, S., and Ramesh, R.: Intra-event isotope and raindrop size data of tropical rain reveal effects concealed by event averaged data, Climate Dynamics, 47, 981–987, https://doi.org/10.1007/s00382-015-2884-7, 2016.

Meyer, A. and Welp, L. R.: Water vapor stable isotope memory effects of common tubing materials, https://doi.org/10.4231/H7ZJ-6J45, 2023.

Muggeo, V. M. R.: segmented: Regression models with break-points / change-Points (with possibly random effects) estimation Version 1.6-0, CRAN [code], https://CRAN.R-project.org/package=segmented, 2022.

Penna, D., Stenni, B., Šanda, M., Wrede, S., Bogaard, T. A., Michelini, M., Fischer, B. M. C., Gobbi, A., Mantese, N., Zuecco, G., Borga, M., Bonazza, M., Sobotková, M., Čejková, B., and Wassenaar, L. I.: Technical Note: Evaluation of between-sample memory effects in the analysis of δ^2H and $\delta^{18}O$ of water samples measured by laser spectroscopes, Hydrology and Earth System Sciences, 16, 3925–3933, https://doi.org/10.5194/hess-16-3925-2012, 2012.

Electrical properties of plastic materials: https://www.professionalplastics.com/professionalplastics/ElectricalPropertiesofPlastics.pdf, last access: 17 December 2021.

Salmon, O. E., Welp, L. R., Baldwin, M. E., Hajny, K. D., Stirm, B. H., and Shepson, P. B.: Vertical profile observations of water vapor deuterium excess in the lower troposphere, Atmospheric Chemistry and Physics, 19, 11525–11543, https://doi.org/10.5194/acp-19-11525-2019, 2019.

Schmidt, M., Maseyk, K., Lett, C., Biron, P., Richard, P., Bariac, T., and Seibt, U.: Concentration effects on laser-based $\delta^{18}O$ and δ^2H measurements and implications for the calibration of vapour measurements with liquid standards, Rapid Commun. Mass Spectrom., 24, 3553–3561, https://doi.org/10.1002/rcm.4813, 2010.

Sodemann, H., Aemisegger, F., Pfahl, S., Bitter, M., Corsmeier, U., Feuerle, T., Graf, P., Hankers, R., Hsiao, G., Schulz, H., Wieser, A., and Wernli, H.: The stable isotopic composition of water vapour above Corsica during the HyMeX SOP1 campaign: insight into vertical mixing processes from lower-tropospheric survey flights, Atmos. Chem. Phys., 17, 6125–6151, https://doi.org/10.5194/acp-17-6125-2017, 2017.

Sturm, P. and Knohl, A.: Water vapor δ^2H and $\delta^{18}O$ measurements using off-axis integrated cavity output spectroscopy, Atmos. Meas. Tech., 3, 67–77, https://doi.org/10.5194/amt-3-67-2010, 2010.

Toson, P., Doshi, P., and Jajcevic, D.: Explicit residence time distribution of a generalised cascade of continuous stirred tank reactors for a description of short recirculation time (bypassing), Processes, 7, 615, https://doi.org/10.3390/pr7090615, 2019.

Tremoy, G., Vimeux, F., Cattani, O., Mayaki, S., Souley, I., and Favreau, G.: Measurements of water vapor isotope ratios with wavelength-scanned cavity ring-down spectroscopy technology: new insights and important caveats for deuterium excess measurements in tropical areas in comparison with isotope-ratio mass spectrometry, Rapid Communications in Mass Spectrometry, 25, 3469–3480, https://doi.org/10.1002/rcm.5252, 2011.

Vallet-Coulomb, C., Couapel, M., and Sonzogni, C.: Improving memory effect correction to achieve high-precision analysis of $\delta^{17}O$, $\delta^{18}O$, δ^2H, ^{17}O-excess and d-excess in water using cavity ring-down laser spectroscopy, Rapid Communications in Mass Spectrometry, 35, e9108, https://doi.org/10.1002/rcm.9108, 2021.

595 Webster, C. R. and Heymsfield, A. J.: Water isotope ratios D/H, $^{18}O/^{16}O$, $^{17}O/^{16}O$ in and out of clouds map dehydration pathways, Science, 302, 1742–1745, https://doi.org/10.1126/science.1089496, 2003.

Zannoni, D., Steen-Larsen, H. C., Peters, A. J., Wahl, S., Sodemann, H., and Sveinbjörnsdóttir, A. E.: Non-equilibrium fractionation factors for D/H and $^{18}O/^{16}O$ during oceanic evaporation in the north-west Atlantic region, Journal of Geophysical Research: Atmospheres, 127, e2022JD037076, https://doi.org/10.1029/2022JD037076, 2022.